Chemical Science

ROYAL SOCIETY OF CHEMISTRY

EDGE ARTICLE

View Article Online
View Journal | View Issue

Cite this: *Chem. Sci.*, 2021, **12**, 8157

All publication charges for this article have been paid for by the Royal Society of Chemistry

Transition-metal-like bonding behaviors of a boron atom in a boron-cluster boronyl complex $[(\eta^7\text{-}B_7)\text{-}B\text{-}BO]^-$†

Wen-Juan Tian, ‡[a] Wei-Jia Chen,‡[b] Miao Yan,[a] Rui Li,[a] Zhi-Hong Wei,[a] Teng-Teng Chen,[b] Qiang Chen,[a] Hua-Jin Zhai, *[a] Si-Dian Li *[a] and Lai-Sheng Wang *[b]

Boron displays many unusual structural and bonding properties due to its electron deficiency. Here we show that a boron atom in a boron monoxide cluster (B_9O^-) exhibits transition-metal-like properties. Temperature-dependent photoelectron spectroscopy provided evidence of the existence of two isomers for B_9O^-: the main isomer has an adiabatic detachment energy (ADE) of 4.19 eV and a higher energy isomer with an ADE of 3.59 eV. The global minimum of B_9O^- is found surprisingly to be an umbrella-like structure (C_{6v}, $^1A_1$) and its simulated spectrum agrees well with that of the main isomer observed. A low-lying isomer (C_s, $^1A'$) consisting of a BO unit bonded to a disk-like B_8 cluster agrees well with the 3.59 eV ADE species. The unexpected umbrella-like global minimum of B_9O^- can be viewed as a central boron atom coordinated by a η^7-B_7 ligand on one side and a BO ligand on the other side, $[(\eta^7\text{-}B_7)\text{-}B\text{-}BO]^-$. The central B atom is found to share its valence electrons with the B_7 unit to fulfill double aromaticity, similar to that in half-sandwich $[(\eta^7\text{-}B_7)\text{-}Zn\text{-}CO]^-$ or $[(\eta^7\text{-}B_7)\text{-}Fe(CO)_3]^-$ transition-metal complexes. The ability of boron to form a half-sandwich complex with an aromatic ligand, a prototypical property of transition metals, brings out new metallomimetic properties of boron.

Received 28th January 2021
Accepted 29th April 2021

DOI: 10.1039/d1sc00534k

rsc.li/chemical-science

1. Introduction

The electron deficiency of boron leads to unusual structures and bonding in bulk boron,[1] boron compounds,[2–4] and size-selected boron clusters.[5–8] One interesting emerging property that has been recognized in recent years is the "metal-lomimetic" properties of boron,[9] manifested most dramatically in a stable borylene dicarbonyl complex, in which two CO ligands are coordinated to a monovalent boron *via* donor–acceptor bonds.[10] The formation of carbonyl complexes is one of the most prototypical chemical properties of transition metals, because of their partially filled d-shells. The partially-filled 2p orbitals endowed boron with similar properties. Even though borane compounds are well-known Lewis acids to form donor–acceptor complexes due to the electron deficiency of boron, carbonyls in the new boron metallomimetics have been found to display similar chemical reactivities to those in transition metal carbonyls.[11,12] Another iconic chemical property of transition metals is the formation of sandwich or half-sandwich complexes with aromatic arene ligands.[13] The interactions between the d orbitals and the π orbitals of the aromatic ligands provide exceptional stabilities for the transition-metal sandwich compounds.[14] In the current article, we report a boron-cluster boronyl complex, $[(\eta^7\text{-}B_7)\text{-}B\text{-}BO]^-$, featuring a central boron atom that exhibits the two most important bonding properties of a transition metal atom, *i.e.*, complexation by a CO analogue of the boronyl ligand (BO^-) and an arene-analog of the doubly aromatic B_7 motif.

During the past two decades, extensive joint experimental and theoretical investigations have revealed that most size-selected boron cluster monoanions B_n^- possess 2D structures for $n = 3$–38, 40–42,[5–8] even though 3D borospherene cages have been observed for B_{40}^- and B_{39}^-,[15] minor seashell-like isomers observed for B_{28}^- and B_{29}^-,[16] and a well-defined bilayer global minimum observed recently for B_{48}^-.[17] The most interesting finding is the chemical bonding in the planar boron clusters, which is characterized by both delocalized σ and π bonds.[18] The delocalized π bonds in the planar boron clusters are found to be similar to those in polycyclic aromatic hydrocarbons, leading to the concept of hydrocarbon analogues of boron clusters.[19] One of the most prototypical planar boron cluster is B_9^-, which was found to have a D_{8h} wheel-like structure with a central B atom inside a B_8 ring (B©B_8).[20] Chemical bonding analyses revealed that the B_9^- cluster is bonded by eight two-center two-electron

[a]*Nanocluster Laboratory, Institute of Molecular Science, Shanxi University, Taiyuan 030006, China. E-mail: hj.zhai@sxu.edu.cn; lisidian@sxu.edu.cn*

[b]*Department of Chemistry, Brown University, Providence, Rhode Island 02912, USA. E-mail: lai-sheng_wang@brown.edu*

† Electronic supplementary information (ESI) available. See DOI: 10.1039/d1sc00534k

‡ These authors contributed equally to this work.

(2c–2e) σ bonds on its periphery, whereas the central boron atom is bonded with the B_8 ring *via* three delocalized 9c–2e σ bonds and three delocalized 9c–2e π bonds, making B_9^- a doubly aromatic system since both the σ and π electron systems satisfy the $(4N + 2)$ Hückel rule. It was further found that the central B atom can be replaced by a transition metal to form a novel class of doubly aromatic borometallic wheel clusters, $M©B_n^-$ for $n = 8$–10.[21] In fact, the central B atom in the D_{8h} B_9^- cluster can be viewed as having transition-metal-like bonding properties. The B_8 cluster was found to have a D_{7h} wheel structure with a triplet ground state.[20a] Adding two electrons to B_8 resulted in a closed-shell doubly aromatic B_8^{2-} species,[22] similar to B_9^-. Subsequently, the B_7^- cluster was found to have a triplet C_{6v} concave structure because the B_6 ring is too small to host the central B atom.[23] Adding two electrons to B_7^- led to a closed-shell doubly aromatic B_7^{3-} unit, first realized in the half-sandwich B_7Pr cluster, *i.e.* $[(\eta^7\text{-}B_7)\text{-}Pr^{III}]$.[24] A number of binary clusters containing the aromatic B_7^{3-} unit have been computed recently.[25]

Here we report a joint photoelectron spectroscopy (PES) and quantum chemical study of the B_9O^- cluster. Temperature-dependent PES experiments suggested that two isomers contributed to the well-resolved photoelectron spectra. Global minimum searches found that the most stable isomer of B_9O^- has an unexpected 3D umbrella-like structure **1** (C_{6v}, $^1A_1$), along with two other low-lying isomers, a disk-like structure with a BO unit bonded to the edge of a 2D B_8 cluster **2** (C_s, $^1A'$) and a double-chain-shaped structure **3** (C_s, $^1A'$). The simulated spectra of structures **1** and **2** together agree well with the experimental data. The global minimum C_{6v} umbrella structure of B_9O^- consists of an unprecedented central B atom being sandwiched by a BO boronyl ligand and a η^7-B_7 aromatic ligand, *i.e.* $[(\eta^7\text{-}B_7)\text{-}B\text{-}BO]^-$. Comparisons of the bonding in the C_{6v} B_9O^- with that in $[(\eta^7\text{-}B_7)\text{-}Zn\text{-}CO]^-$, $[(\eta^7\text{-}B_7)\text{-}Fe(CO)_3]^-$ and $[(\eta^7\text{-}B_7)\text{-}Pr]$ provide evidence for transition-metal-like bonding behaviors by the central B atom, which shares its valence electrons with the B_7 ligand to achieve double aromaticity.

2. Experimental and theoretical methods

2.1 Photoelectron spectroscopy

The experiment was carried out using a magnetic-bottle PES apparatus equipped with a laser vaporization cluster source, details of which have been described before.[6,26] The B_9O^- clusters were produced by laser vaporization of a mixed Bi/^{10}B target. The B_9O^- clusters were formed in the nozzle due to residual oxygen impurity on the target surface. The clusters were formed in a large waiting room nozzle,[6,26] which were entrained by a He carrier gas seeded with 5% Ar and cooled *via* supersonic expansion. After passing a skimmer, negatively-charged clusters were extracted perpendicularly from the collimated cluster beam into a time-of-flight mass spectrometer for size analyses. The B_9O^- clusters of interest were mass-selected and decelerated before photodetachment. Two photon energies were used in the PES experiment: 266 nm (4.661 eV) from a Nd:YAG laser and 193 nm (6.424 eV) from an ArF excimer laser. Photoelectron spectra were calibrated using the known spectra of Bi^-. The resolution of the PES apparatus was $\Delta E_k/E_k \approx 2.5\%$, *i.e.* ~25 meV for 1 eV electrons.

As shown previously,[6,27] the cluster cooling efficiency in our experiment depends on their residence times inside the large waiting room nozzle. The clusters that leave the nozzle later are colder than those that leave earlier. Thus, the cluster temperatures can be controlled to a limited degree by selecting the appropriate timing for cluster extraction into the time-of-flight mass spectrometer, as shown in the spectra in Fig. S1.†

2.2 Theoretical methods

The global minimum search was conducted at the density-functional theory (DFT) level using the Coalescence Kick (CK) algorithm,[28] aided with manual structural constructions. About 4000 stationary points for B_9O^-, and the same number of points for B_9O, were probed in the CK search. Candidate low-lying structures were then fully optimized at the B3LYP/6-311++G(d,p)[29] and PBE0/6-311++G(d,p)[30] levels, respectively. Adiabatic (ADEs) and vertical (VDEs) detachment energies were calculated at the B3LYP level for the ground state transition and at the time-dependent B3LYP (TD-B3LYP)[31] level for higher VDEs. Single-point coupled-cluster calculations (CCSD(T))[32,33] were also performed at the B3LYP geometries to refine the ground state ADEs and VDEs and to further evaluate the relative energies of the low-lying structures. The ADE was calculated as the energy difference between the optimized anion and neutral for each isomer, whereas the first VDE was calculated as the energy difference between the anion and neutral at the anion geometry. Higher VDEs were calculated at the B3LYP level using TD-DFT. Chemical bonding was analyzed using both MOs and adaptive natural density partitioning (AdNDP).[34] Orbital compositions were analyzed using Muitiwfn.[35] All calculations were carried out using Gaussian 09.[36]

3. Experimental results

The photoelectron spectra of B_9O^- were obtained at two photon energies, 266 nm and 193 nm, as shown in Fig. 1. The 266 nm spectrum (Fig. 1a) displays three well-resolved bands. Band X′ at the low binding energy side is relatively broad with a VDE of 3.69 eV measured from the band maximum. There are hints of vibrational structures in band X′, but they are not well resolved.

Hence, we determined the ADE by drawing a straight line at its leading edge and then adding the instrumental resolution. The ADE so measured is 3.59 eV, which also represents the electron affinity (EA) of B_9O. Band X at a VDE of 4.22 eV and band A at a VDE of 4.31 eV are relatively sharp and closely spaced. The ADE for band X was estimated to be 4.19 eV from its leading edge. At 193 nm (Fig. 1b), several more PES bands were observed beyond 4.7 eV, including two well-resolved bands A′ (VDE: 4.86 eV) and B′ (VDE: 5.28 eV). The signal-to-noise ratios in the higher binding energy range are poor, but a broad band around ~5.9 eV is discernible which may contain multiple

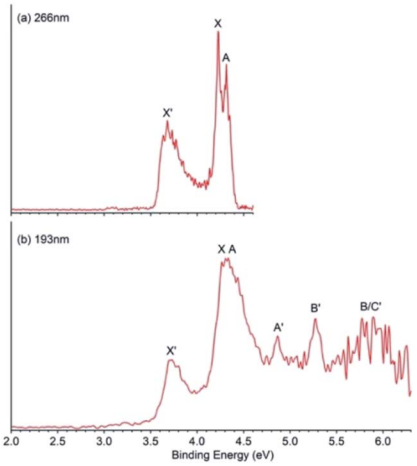

Fig. 1 Photoelectron spectra of B_9O^- at (a) 266 nm (4.661 eV) and (b) 193 nm (6.424 eV).

detachment transitions. It is labeled as B/C′ for the sake of discussion.

Even though the PES features of B_9O^- are well resolved, the spectra appear more complicated in comparison to those of B_8^- or B_9^-,[20] suggesting possible existence of multiple isomers as observed for those of B_7^-.[23] As shown previously,[6,27] we could tune the cluster temperatures to a limited degree by varying the residence time of the clusters inside the nozzle. Indeed, as we varied the experimental conditions, we found that the relative intensities of the spectral features changed, providing direct evidence of the existence of isomers in the cluster beam. As shown in Fig. S1,† the relative intensities of bands X′, A′, and B′ increased under hotter source conditions, suggesting they came from a slightly higher energy isomer of B_9O^- with an EA of 3.59 eV for the corresponding neutral B_9O isomer. Bands X and A and possibly some features around 5.9 eV should belong to a lower energy isomer of B_9O^- with an EA of 4.19 eV for the corresponding B_9O isomer. The temperature-dependent data are critical for the spectral assignments and comparison with theoretical calculations. All the observed VDEs are given in Table 1, where they are compared with the theoretical results to be discussed below.

4. Theoretical results

Our global minimum searches identified several low-lying isomers, as shown in Fig. 2. Other higher-lying optimized geometries and their relative energies at the B3LYP,[29] PBE0,[30] and single-point CCSD(T)//B3LYP[32,33] levels are given in Fig. S2 and S3 in the ESI.† As shown previously,[37–39] all boron-rich oxide clusters contain the highly stable boronyl (BO) ligand,[40] which is isoelectronic with CN. Similarly, we found that the three lowest-lying isomers of $B_9O^{0/-}$ all contain the BO unit bonded to a B_8 cluster (Fig. 2). The global minimum of B_9O^- (**1**) at all three levels of theory is a closed-shell 3D umbrella-like structure with C_{6v} symmetry. The second lowest-lying isomer (**2**) consists of a disk-like B_8 cluster bonded to a BO unit, which is 0.13 eV higher in energy than the C_{6v} structure at the B3LYP level, 0.79 eV higher at the PBE0 level, and 0.62 eV higher at the CCSD(T) level. The next isomer (**3**) is 0.12 eV higher in energy than the C_{6v} global minimum at the B3LYP level, but much higher in energy at the PBE0 level by 1.14 eV and the CCSD(T) level by 0.85 eV.

The low-lying isomers of the B_9O neutral are similar to those of the anions (Fig. 2), except that the energy differences between the isomers become much smaller. In fact, the neutral isomers **1′** and **2′** are almost isoenergetic at the CCSD(T) level. The

Table 1 Experimental VDEs compared with the calculated values for the three lowest-lying isomers (**1–3**) of B_9O^- at the TD-B3LYP level of theory. All energies are in eV

Features	VDE (exp)[a]	Final state and electronic configuration	VDE (theo)
C_{6v} B_9O^- (**1**)			
X	4.22	$^2E_1\{\ldots(6a_1)^2(1b_1)^2(3e_1)^4(4e_1)^3\}$	4.21
A	4.31	$^2E_1\{\ldots(6a_1)^2(1b_1)^2(3e_1)^4(4e_1)^3\}$	4.37
B	∼5.9	$^2E_1\{\ldots(6a_1)^2(1b_1)^2(3e_1)^3(4e_1)^4\}$	5.84
		$^2E_1\{\ldots(6a_1)^2(1b_1)^2(3e_1)^3(4e_1)^4\}$	5.85
		$^2B_1\{\ldots(6a_1)^2(1b_1)^1(3e_1)^4(4e_1)^4\}$	6.25
C_s B_9O^- (**2**)			
X′	3.69	$^2A''\{\ldots(9a')^2(4a'')^2(10a')^2(5a'')^2(11a')^2(6a'')^1\}$	3.50
A′	4.86	$^2A''\{\ldots(9a')^2(4a'')^2(10a')^2(5a'')^2(11a')^1(6a'')^2\}$	4.76
B′	5.28	$^2A'\{\ldots(9a')^2(4a'')^2(10a')^2(5a'')^1(11a')^2(6a'')^2\}$	5.17
C′	∼5.9	$^2A''\{\ldots(9a')^2(4a'')^2(10a')^1(5a'')^2(11a')^2(6a'')^2\}$	5.79
C_s B_9O^- (**3**)			
X′	3.69	$^2A'\{\ldots(2a'')^2(11a')^2(12a')^2(13a')^2(3a'')^2(14a')^1\}$	3.56
A′	4.86	$^2A''\{\ldots(2a'')^2(11a')^2(12a')^2(13a')^2(3a'')^1(14a')^2\}$	4.79
B′	5.28	$^2A'\{\ldots(2a'')^2(11a')^2(12a')^2(13a')^1(3a'')^2(14a')^2\}$	5.35
C′	∼5.9	$^2A'\{\ldots(2a'')^2(11a')^2(12a')^1(13a')^2(3a'')^2(14a')^2\}$	5.54
		$^2A'\{\ldots(2a'')^2(11a')^1(12a')^2(13a')^2(3a'')^2(14a')^2\}$	5.65

[a] The estimated experimental uncertainty is ±0.02 eV.

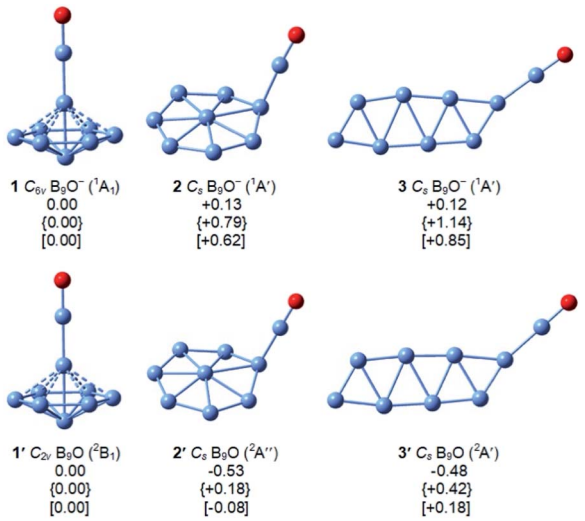

Fig. 2 The structures of the three lowest-lying isomers of B_9O^- (**1–3**) and B_9O (**1′–3′**) at the B3LYP/6-311++G(d,p) level. Their relative energies in eV are given at the B3LYP/6-311++G(d,p), PBE0/6-311++G(d,p) (in curly brackets), and single-point CCSD(T)//B3LYP/6-311++G(d,p) (in square brackets) levels, respectively.

detailed structural parameters at the B3LYP level for the three low-lying structures of $B_9O^{0/-}$ are given in Fig. S4.† The umbrella-like global minimum (**1′**) is distorted to C_{2v} symmetry due to the Jahn–Teller effect.

5. Comparison between experiment and theory

To confirm the global minimum of B_9O^- and help assign the two observed isomers in the experiment, we calculated the ADEs and VDEs for the three low-lying isomers of B_9O^- at the B3LYP and single-point CCSD(T) levels of theory. The ground state ADE and VDE for each isomer are compared with the experimental data in Table 2. We found that both B3LYP and CCSD(T) gave similar results. The calculated ADE and VDE for the umbrella isomer **1** are significantly higher than those for isomers **2** and **3**. The computed ADE/VDE values of 4.15/4.30 eV for isomer **1** at the CCSD(T) level are in excellent agreement with the experimental observation of 4.19/4.22 eV for the X band. On the other hand, the computed first ADE/VDE for isomers **2** and **3** are similar and both [3.45/3.58 eV for **2** and 3.48/3.62 eV for **3** at the CCSD(T) level] seem to agree well with the experimental observation of 3.59/3.69 eV for the X′ band. Thus, even though isomer **3** is higher in energy, the first ADE and VDE are not sufficient to rule it out.

The higher VDEs for all three isomers are compared with the experimental data in Table 1, with the final electron configurations and electronic states of the corresponding neutrals indicated. The valence molecular orbital (MO) pictures are shown in Fig. S5–S7† for isomers **1–3**, respectively. Because all three isomers are closed-shell, detachment from each occupied MO is expected to give a single PES band, resulting in relatively simple photoelectron spectra and facilitating comparisons with the experimental data. Each detachment channel was fitted with a unit-area Gaussian with a width of 0.04 eV to produce a simulated spectrum. The simulated spectra for isomers **1–3** using the data at the B3LYP level of theory are compared with the 193 nm spectrum in Fig. 3. The calculated VDEs for the first two detachment channels of isomer **1** are close to each other, consistent with the X and A bands. The calculated VDEs for the third and fourth detachment channels of isomer **1** are almost identical and they must contribute to the broad band at ~5.9 eV. The fifth detachment channel with a computed VDE of 6.25 eV is near the cutoff energy of the 193 nm spectrum, where the spectral signal-to-noise ratios were poor. The overall good agreement between the simulated spectrum for isomer **1** and the observed PES bands X, A, and B provides considerable credence for the C_{6v} umbrella structure as the global minimum of B_9O^-.

As shown in Table 1 and Fig. 3, the first three detachment channels of both isomers **2** and **3** agree well with the observed X′, A′, and B′ bands. The fourth detachment channel of isomer **2** is also in good agreement with the broad feature at ~5.9 eV. However, the computed VDEs for the fourth and fifth detachment channels of isomer **3** do not agree with the experimental observation and thus it can be ruled out as the carrier for the observed X′, A′, and B′ bands. This conclusion is also consistent with the relatively high energy of isomer **3**. Hence, both the experimental and theoretical results indicate that the co-existing low-lying isomer in the cluster beam of B_9O^- should be isomer **2**.

6. Discussion

6.1 The structures and chemical bonding of B_9O^-

The 3D umbrella global minimum structure for B_9O^- is both surprising and unprecedented. Several boron monoxide clusters have been studied experimentally before and they are all found to consist of a planar boron cluster motif bonded to a BO

Table 2 Comparison of the first experimental ADE and VDE with those calculated at the B3LYP/6-311++G(d,p) and single-point CCSD(T)//B3LYP/6-311++G(d,p) levels of theory for the three lowest-lying isomers of B_9O^-. All energies are in eV

		ADE (theo)		VDE (theo)			
Isomers	Final state	B3LYP	CCSD(T)	B3LYP	CCSD(T)	ADE (exp)	VDE (exp)
1, C_{6v}	^2A	4.08	4.15	4.21	4.30	4.19 ± 0.04	4.22 ± 0.02
2, C_s	$^2A''$	3.38	3.45	3.50	3.58	3.59 ± 0.04	3.69 ± 0.02
3, C_s	$^2A'$	3.44	3.48	3.56	3.62		

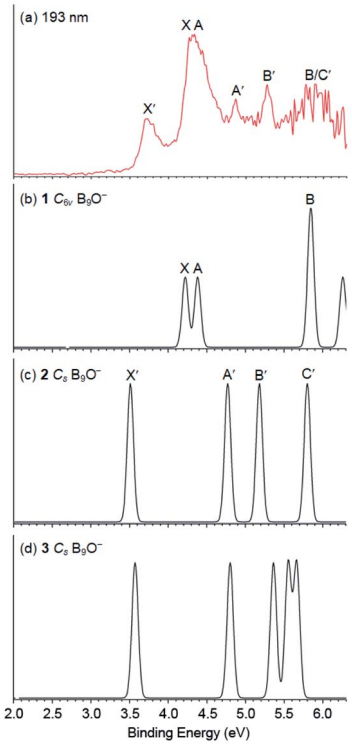

Fig. 3 Comparison of (a) the photoelectron spectrum of B_9O^- at 193 nm with the simulated spectra of (b) C_{6v} (**1**), (c) C_s (**2**) and (d) C_s (**3**) at the TD-B3LYP level. The simulated spectra were obtained by fitting the calculated VDEs with unit-area Gaussian functions of 0.04 eV width.

unit on the periphery due to the exceptional stability of the boronyl unit.[39] The boron cluster motifs in these monoxide clusters are usually related to the most stable pure boron clusters, such as isomer **2** for B_9O^-, which we expected to be the global minimum. It should be pointed out that the structures of the B_9O cluster were studied previously using DFT methods.[38] The most stable structure reported was similar to isomer **3** of the current study both as a neutral and anion. Two other low-lying structures were also identified in previous studies, one is similar to the fourth isomer of B_9O^- (C_s, $^1A'$) which is 0.22 eV above the C_{6v} global minimum at the B3LYP level and the other one is similar to the eleventh isomer of B_9O^- (C_{2v}, $^1A_1$) which is 1.45 eV above the global minimum at the B3LYP level (Fig. S2†). Even though these structures are low-lying isomers in the neutral (Fig. S3†), they are significantly higher in energy in the anion.

The most unusual structural feature of the umbrella global minimum of B_9O^- is the central boron atom. It forms a σ bond with the BO unit, but its bonding to the B_7 unit is unprecedented. The B–B distances between this atom and the periphery of the B_7 unit are 1.91 Å, significantly longer than the B–B distance (1.72 Å) between the apex B atom of the B_7 unit and the six peripheral B atoms (Fig. S4†). To understand the stability and bonding of the umbrella structure of B_9O^-, we carried out AdNDP analyses,[34] as shown in Fig. 4. The triple bond in the BO unit (Fig. 4a), the σ bond between the central B and the BO unit (Fig. 4d), and the six 2c–2e bonds for the periphery of the B_7 motif (Fig. 4b) are clearly

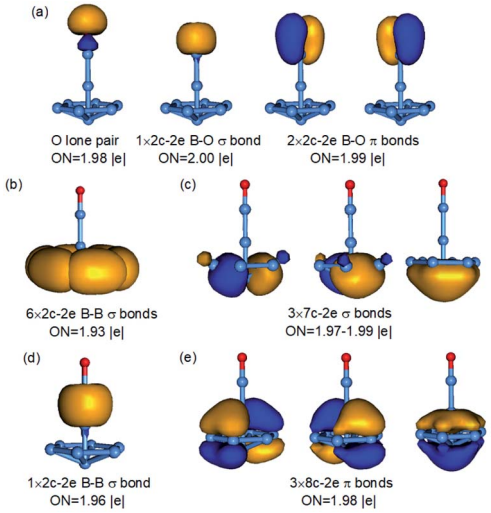

Fig. 4 AdNDP bonding analyses for the C_{6v} B_9O^- global minimum. The different bonding elements are given in (a–e). ON is the occupation number.

revealed. The most interesting bonding features are the two sets of three delocalized σ and π bonds (Fig. 4c and e), which are almost identical to those in the B_7^{3-} motif found in the [(η^7-B_7)-Pr] cluster.[24] This observation suggests that the central B atom shares its valence electrons with the B_7 unit to fulfill double aromaticity. Thus, it is the exceptional stability of the doubly aromatic B_7^{3-} system that gives rise to the extraordinary stability of the unexpected umbrella global minimum for B_9O^-. The extremely high electron binding energy (4.19 eV) of the umbrella structure indicates its high electronic stability. The HOMO (e_1) of the C_{6v} B_9O^- (Fig. S5†) is doubly degenerate and corresponds to two orbitals responsible for the σ aromaticity. Thus, the removal of an electron from the HOMO not only induces a symmetry breaking in neutral B_9O (C_{2v}) due to the Jahn–Teller effect, but also decreases the σ aromaticity in the B_7 motif, which explains why the stability of the umbrella structure in the neutral (**1′** in Fig. 2) is reduced relative to isomers **2′** and **3′**. Even though charge transfer is not expected from the central B atom to the B_7 unit, the umbrella structure of B_9O^- can be approximately viewed as an η^7-B_7^{3-} ligand coordinated to a B^{II} center or [(η^7-B_7)-B^{II}-BO]$^-$.

We also analyzed the bonding in isomers **2** and **3** of B_9O^- using AdNDP, as displayed in Fig. S8 and S9,† respectively. Each can be described as a BO unit bonded to a B_8 motif. In isomer **2**, the disk-shaped B_8 motif is similar to the global minimum D_{7h} B_8.[20] The B_8 unit still maintains σ aromaticity, but it is π anti-aromatic with only two π bonds, consistent with its structural distortion. Isomer **3** contains two delocalized σ and two delocalized π bonds, which can be viewed as doubly antiaromatic in agreement with the fact that it is not energetically competitive relative to isomers **1** and **2**.

6.2 Comparison of the bonding in C_{6v} B_9O^- with transition metal complexes

The high stability of the doubly aromatic B_7^{3-} unit, first realized in the [(η^7-B_7)-Pr] cluster,[24] is interesting. It has been used

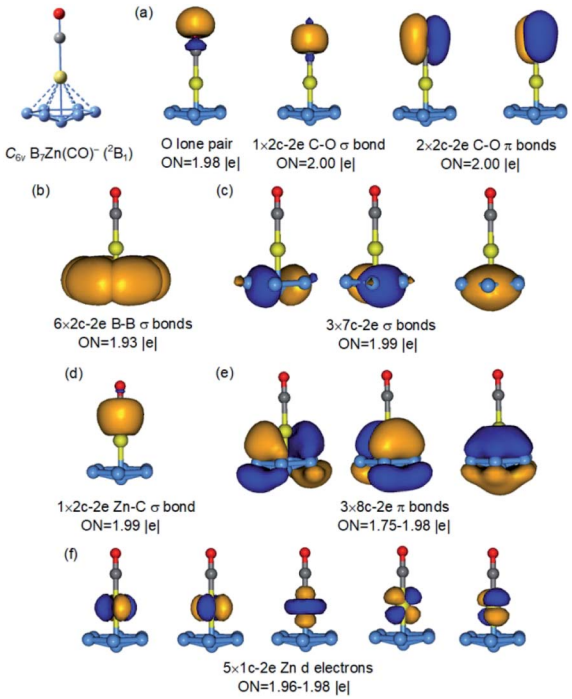

Fig. 5 AdNDP bonding analyses for the C_{6v} $B_7Zn(CO)^-$ complex. ON is the occupation number.

recently to design binary clusters with alkali or alkali earth elements,[25] which can transfer charges more easily to the B_7 motif. In particular, the B_7^{3-} ligand has been utilized to stabilize the single σ bond in Mg_2^{2+} or Zn_2^{2+} in $B_7M_2^-$ type clusters.[25a,b] The bonding mode of the η^7-B_7 unit to the central B atom in the C_{6v} B_9O^- cluster is reminiscent of the coordination mode of arenes to transition metals in sandwich or half-sandwich complexes.[13,14] Thus, the C_{6v} B_9O^- cluster brings out a new metallomimetic property of boron. To further understand this metallomimetic property, we compare the bonding in the C_{6v} B_9O^- cluster with that of two model metal complexes, $[(\eta^7\text{-}B_7)\text{-Zn-CO}]^-$ and $[(\eta^7\text{-}B_7)\text{-Fe(CO)}_3]^-$, as shown in Fig. 5 and S10,† respectively.

Because the 3d electrons of Zn do not participate in bonding, the $[(\eta^7\text{-}B_7)\text{-Zn-CO}]^-$ complex can be considered as isoelectronic to $[(\eta^7\text{-}B_7)\text{-B-BO}]^-$ and their bonding is nearly identical. As shown in Fig. S10,† the bonding between the η^7-B_7 motif with Fe in $[(\eta^7\text{-}B_7)\text{-Fe(CO)}_3]^-$ is also similar to that in the C_{6v} B_9O^- cluster (Fig. 4). In fact, the 18-electron rule is fulfilled in $[(\eta^7\text{-}B_7)\text{-Fe(CO)}_3]^-$, making it a highly stable species isoelectronic to the well-known $(\eta^6\text{-}C_6H_6)$–$Cr(CO)_3$ complex.[14] To further demonstrate the analogy between the BO^- and CO ligands,[41] we also analysed the bonding in $[(\eta^7\text{-}B_7)\text{-B-CO}]$ by replacing the BO^- ligand in the C_{6v} B_9O^- cluster with CO. As shown in Fig. S12,† the bonding in this model complex is identical to that in $[(\eta^7\text{-}B_7)\text{-B-BO}]^-$. Thus, the central B atom in $[(\eta^7\text{-}B_7)\text{-B-BO}]^-$ can be considered to embody the two most important bonding properties of transition metals, the ability to form carbonyl complexes and sandwich-type complexes with aromatic arenes. While half-sandwich complexes of planar aromatic boron clusters with transition metal atoms have been observed or proposed,[42,43] the discovery of the half-sandwich complex between B_7 and the B atom is unprecedented, suggesting again the versatility of the chemical bonding of boron.

7. Conclusions

In conclusion, we have investigated the structures and bonding of a boron monoxide cluster B_9O^- using photoelectron spectroscopy and theoretical calculations. Temperature-dependent experiments revealed the existence of two isomers in the photoelectron spectra, one with an EA of 3.59(4) eV and another with an EA of 4.19(4) eV for the corresponding B_9O neutrals. The global minimum of B_9O^- is found surprisingly to have a 3D C_{6v} umbrella-like structure, corresponding to the high EA species, whereas a low-lying isomer consisting of a BO unit bonded to the periphery of a disk-like B_8 motif is found to correspond to the low EA species. The C_{6v} global minimum can be viewed as a half-sandwich complex with the central B atom coordinated by a η^7-B_7 unit and a BO unit, *i.e.* $[(\eta^7\text{-}B_7)\text{-B-BO}]^-$. Chemical bonding analyses showed that the central B atom shares its valence electrons with the B_7 unit to fulfill double aromaticity, which provides the exceptional stability for the unprecedented 3D global minimum of the B_9O^- cluster. Comparison of the bonding in the C_{6v} B_9O^- cluster with that in $[(\eta^7\text{-}B_7)\text{-Pr}]$, as well as in model complexes $[(\eta^7\text{-}B_7)\text{-Zn-CO}]^-$, $[(\eta^7\text{-}B_7)\text{-Fe(CO)}_3]^-$, and $[(\eta^7\text{-}B_7)\text{-B-CO}]$ suggest that the central B atom in $[(\eta^7\text{-}B_7)\text{-B-BO}]^-$ behaves like transition metals in its bonding to the aromatic B_7 unit and the BO^- ligand.

Conflicts of interest

There are no conflicts to declare.

Acknowledgements

The experimental work carried out at Brown University was supported by the U.S. National Science Foundation (CHE-2053541 to L. S. W.). Theoretical work carried out at Shanxi University was supported by the National Science Foundation of China (21873058 and 21573138 to H. J. Z.; 21720102006 to S. D. L.), the Scientific Research Startup Fund of Shanxi University (203545048 to W. J. T) and the Applied Basic Research Programs of Natural Science Foundation of Shanxi Province (201901D211147 to W. J. T).

Notes and references

1 B. Albert and H. Hillebrecht, *Angew. Chem., Int. Ed.*, 2009, **48**, 8640–8668.
2 W. N. Lipscomb, *Science*, 1977, **196**, 1047–1055.
3 E. D. Jemmis, M. M. Balakrishnarajan and P. D. Pancharatna, *Chem. Rev.*, 2002, **102**, 93–144.
4 H. Braunschweig, R. D. Dewhurst and V. H. Gessner, *Chem. Soc. Rev.*, 2013, **42**, 3197–3208.
5 A. N. Alexandrova, A. I. Boldyrev, H. J. Zhai and L. S. Wang, *Coord. Chem. Rev.*, 2006, **250**, 2811–2866.

6 L. S. Wang, *Int. Rev. Phys. Chem.*, 2016, **35**, 69–142.
7 S. Pan, J. Barroso, S. Jalife, T. Heine, K. R. Asmis and G. Merino, *Acc. Chem. Res.*, 2019, **52**, 2732–2744.
8 T. Jian, X. Chen, S. D. Li, A. I. Boldyrev, J. Li and L. S. Wang, *Chem. Soc. Rev.*, 2019, **48**, 3550–3591.
9 M.-A. Legare, C. Pranckevicius and H. Braunschweig, *Chem. Rev.*, 2019, **119**, 8231–8261.
10 (*a*) H. Braunschweig, R. D. Dewhurst, F. Hupp, M. Nutz, K. Radacki, C. W. Tate, A. Vargas and Q. Ye, *Nature*, 2015, **522**, 327–330; (*b*) M. A. Celik, R. Sure, S. Klein, R. Kinjo, G. Bertrand and G. Frenking, *Chem.–Eur. J.*, 2012, **18**, 5676–5692.
11 H. Braunschweig, I. Krummenacher, M.-A. Legare, A. Matler, K. Radacki and Q. Ye, *J. Am. Chem. Soc.*, 2017, **139**, 1802–1805.
12 H. Wang, L. Wu, Z. Lin and Z. Xie, *Angew. Chem., Int. Ed.*, 2018, **57**, 8708–8713.
13 G. Wilkinson, M. Rosenblum, M. C. Whiting and R. B. Woodward, *J. Am. Chem. Soc.*, 1952, **74**, 2125–2126.
14 E. L. Muetterties, J. R. Bleeke and E. J. Wucherer, *Chem. Rev.*, 1982, **82**, 499–525.
15 (*a*) H. J. Zhai, Y. F. Zhao, W. L. Li, Q. Chen, H. Bai, H. S. Hu, Z. A. Piazza, W. J. Tian, H. G. Lu, Y. B. Wu, Y. W. Mu, G. F. Wei, Z. P. Liu, J. Li, S. D. Li and L. S. Wang, *Nat. Chem.*, 2014, **6**, 727–731; (*b*) Q. Chen, W. L. Li, Y. F. Zhao, S. Y. Zhang, H. S. Hu, H. Bai, H. R. Li, W. J. Tian, H. G. Lu, H. J. Zhai, S. D. Li, J. Li and L. S. Wang, *ACS Nano*, 2015, **9**, 754–760.
16 (*a*) Y. J. Wang, Y. F. Zhao, W. L. Li, T. Jian, Q. Chen, X. R. You, T. Ou, X. Y. Zhao, H. J. Zhai, S. D. Li, J. Li and L. S. Wang, *J. Chem. Phys.*, 2016, **144**, 064307; (*b*) H. R. Li, T. Jian, W. L. Li, C. Q. Miao, Y. J. Wang, Q. Chen, X. M. Luo, K. Wang, H. J. Zhai, S. D. Li and L. S. Wang, *Phys. Chem. Chem. Phys.*, 2016, **18**, 29147–29155.
17 W. J. Chen, Y. Y. Ma, T. T. Chen, M. Z. Ao, D. F. Yuan, Q. Chen, X. X. Tian, Y. W. Mu, S. D. Li and L. S. Wang, *Nanoscale*, 2021, **13**, 3868–3876.
18 (*a*) A. P. Sergeeva, I. A. Popov, Z. A. Piazza, L. W. Li, C. Romanescu, L. S. Wang and A. I. Boldyrev, *Acc. Chem. Res.*, 2014, **47**, 1349–1358; (*b*) A. I. Boldyrev and L. S. Wang, *Phys. Chem. Chem. Phys.*, 2016, **18**, 11589–11605.
19 (*a*) H. J. Zhai, B. Kiran, J. Li and L. S. Wang, *Nat. Mater.*, 2003, **2**, 827–833; (*b*) W. Huang, A. P. Sergeeva, H. J. Zhai, B. B. Averkiev, L. S. Wang and A. I. Boldyrev, *Nat. Chem.*, 2010, **2**, 202–206; (*c*) A. P. Sergeeva, Z. A. Piazza, C. Romanescu, W. L. Li, A. I. Boldyrev and L. S. Wang, *J. Am. Chem. Soc.*, 2012, **134**, 18065–18073.
20 (*a*) H. J. Zhai, A. N. Alexandrova, K. A. Birch, A. I. Boldyrev and L. S. Wang, *Angew. Chem., Int. Ed.*, 2003, **42**, 6004–6008; (*b*) L. L. Pan, J. Li and L. S. Wang, *J. Chem. Phys.*, 2008, **129**, 024302.
21 (*a*) A. C. Romanescu, T. R. Galeev, W. L. Li, A. I. Boldyrev and L. S. Wang, *Angew. Chem., Int. Ed.*, 2011, **50**, 9334–9337; (*b*) W. L. Li, C. Romanescu, T. R. Galeev, Z. A. Piazza, A. I. Boldyrev and L. S. Wang, *J. Am. Chem. Soc.*, 2012, **134**, 165–168; (*c*) T. R. Galeev, C. Romanescu, W. L. Li, L. S. Wang and A. I. Boldyrev, *Angew. Chem., Int. Ed.*, 2012, **51**, 2101–2105; (*d*) A. C. Romanescu, T. R. Galeev, W. L. Li, A. I. Boldyrev and L. S. Wang, *Acc. Chem. Res.*, 2013, **46**, 350–358; (*e*) T. T. Chen, W. L. Li, H. Bai, W. J. Chen, X. R. Dong, J. Li and L. S. Wang, *J. Phys. Chem. A*, 2019, **123**, 5317–5324.
22 A. N. Alexandrova, H. J. Zhai, L. S. Wang and A. I. Boldyrev, *Inorg. Chem.*, 2004, **43**, 3552–3554.
23 A. N. Alexandrova, A. I. Boldyrev, H. J. Zhai and L. S. Wang, *J. Phys. Chem. A*, 2004, **108**, 3509–3517.
24 T. T. Chen, W. L. Li, T. Jian, X. Chen, J. Li and L. S. Wang, *Angew. Chem., Int. Ed.*, 2017, **56**, 6916–6920.
25 (*a*) R. Yu, J. Barroso, M. H. Wang, W. Y. Liang, C. Chen, X. Zarate, M. Orozco-Ic, Z. H. Cui and G. Merino, *Phys. Chem. Chem. Phys.*, 2020, **22**, 12312–12320; (*b*) W. Wang, J. Wang, C. Gong, D. Zhang and X. Zhang, *Chin. J. Chem. Phys.*, 2020, **33**, 578–582; (*c*) Y. J. Wang, L. Y. Feng and H. J. Zhai, *Phys. Chem. Chem. Phys.*, 2019, **21**, 18338–18345.
26 L. S. Wang, H. S. Cheng and J. Fan, *J. Chem. Phys.*, 1995, **102**, 9480–9493.
27 J. Akola, M. Manninen, H. Hakkinen, U. Landman, X. Li and L. S. Wang, *Phys. Rev. B: Condens. Matter Mater. Phys.*, 1999, **60**, R11297–R11300.
28 M. Saunders, *J. Comput. Chem.*, 2004, **25**, 621–626.
29 C. T. Lee, W. T. Yang and R. G. Parr, *Phys. Rev. B: Condens. Matter Mater. Phys.*, 1988, **37**, 785–789.
30 R. Krishnan, J. S. Binkley, R. Seeger and J. A. Pople, *J. Chem. Phys.*, 1980, **72**, 650–654.
31 R. Bauernschmitt and R. Ahlrichs, *Chem. Phys. Lett.*, 1996, **256**, 454–464.
32 R. J. Bartlett and M. Musial, *Rev. Mod. Phys.*, 2007, **79**, 291–352.
33 G. E. Scuseria and H. F. Schaefer, *J. Chem. Phys.*, 1989, **90**, 3700–3703.
34 D. Y. Zubarev and A. I. Boldyrev, *Phys. Chem. Chem. Phys.*, 2008, **10**, 5207–5217.
35 T. Lu and F. W. Chen, *J. Comput. Chem.*, 2012, **33**, 580–592.
36 M. J. Frisch, *et al.*, *Gaussian 09, revision D.01*, Gaussian, Inc., Wallingford, CT, 2009.
37 (*a*) H. J. Zhai, Q. Chen, H. Bai, S. D. Li and L. S. Wang, *Acc. Chem. Res.*, 2014, **47**, 2435–2445; (*b*) H. J. Zhai, S. D. Li and L. S. Wang, *J. Am. Chem. Soc.*, 2007, **129**, 9254–9255; (*c*) S. D. Li, H. J. Zhai and L. S. Wang, *J. Am. Chem. Soc.*, 2008, **130**, 2573–2579; (*d*) H. J. Zhai, J. C. Guo, S. D. Li and L. S. Wang, *ChemPhysChem*, 2011, **12**, 2549–2553; (*e*) H. J. Zhai, Q. Chen, H. Bai, H. G. Lu, W. L. Li, S. D. Li and L. S. Wang, *J. Chem. Phys.*, 2013, **139**, 174301; (*f*) M. T. Nguyen, M. H. Matus, V. T. Ngan, D. J. Grant and D. A. Dixon, *J. Phys. Chem. A*, 2009, **113**, 4895–4909.
38 (*a*) M. L. Drummond, V. Meunier and B. G. Sumpter, *J. Phys. Chem. A*, 2007, **111**, 6539–6551; (*b*) T. B. Tai, M. T. Nguyen and D. A. Dixon, *J. Phys. Chem. A*, 2010, **114**, 2893–2912.
39 (*a*) H. J. Zhai, C. Q. Miao, S. D. Li and L. S. Wang, *J. Phys. Chem. A*, 2010, **114**, 12155–12161; (*b*) Q. Chen, H. J. Zhai, S. D. Li and L. S. Wang, *J. Chem. Phys.*, 2012, **137**, 044307; (*c*) Q. Chen, H. Bai, H. J. Zhai, S. D. Li and L. S. Wang, *J. Chem. Phys.*, 2013, **139**, 044308; (*d*) H. Bai, H. J. Zhai,

S. D. Li and L. S. Wang, *Phys. Chem. Chem. Phys.*, 2013, **15**, 9646–9653.

40 H. J. Zhai, L. M. Wang, S. D. Li and L. S. Wang, *J. Phys. Chem. A*, 2007, **111**, 1030–1035.

41 (*a*) Q. Zhang, W. L. Li, C. Q. Xu, M. Chen, M. Zhou, J. Li, D. M. Andrada and G. Frenking, *Angew. Chem., Int. Ed.*, 2015, **54**, 11078–11083; (*b*) J. Jin, G. Wang and M. Zhou, *J. Phys. Chem. A*, 2018, **122**, 2688–2694.

42 (*a*) I. A. Popov, W. L. Li, Z. A. Piazza, A. I. Boldyrev and L. S. Wang, *J. Phys. Chem. A*, 2014, **118**, 8098–8105; (*b*) J. Czekner, L. F. Cheng, G. S. Kocheril, M. Kulichenko, A. I. Boldyrev and L. S. Wang, *Angew. Chem., Int. Ed.*, 2019, **58**, 8877–8881.

43 (*a*) L. Liu, D. Moreno, E. Osorio, A. C. Castro, S. Pan, P. K. Chattaraj, T. Heine and G. Merino, *RSC Adv.*, 2016, **6**, 27177–27182; (*b*) R. Saha, S. Kar, S. Pan, G. Martinez-Guajardo, G. Merino and P. K. Chattaraj, *J. Phys. Chem. A*, 2017, **121**, 2971–2979; (*c*) L. Zhao, X. Qu, Y. Wang, J. Lv, L. Zhang, Z. Hu, G. Gu and Y. Ma, *J. Phys.: Condens. Matter*, 2017, **29**, 265401; (*d*) Y. Wang, X. Wu and J. Zhao, *J. Cluster Sci.*, 2018, **29**, 847–852; (*e*) B. Chen, W. Sun, X. Kuang, C. Lu, X. Xia, H. Shi and G. L. Gutsev, *Phys. Chem. Chem. Phys.*, 2018, **20**, 30376–30383; (*f*) X. Y. Zhao, X. M. Luo, X. X. Tian, H. G. Lu and S. D. Li, *J. Cluster Sci.*, 2019, **30**, 115–121; (*g*) M. Ren, S. Jin, D. Wei, Y. Jin, Y. Tian, C. Lu and G. L. Gutsev, *Phys. Chem. Chem. Phys.*, 2019, **21**, 21746–21752.